Electroluminescence and photoluminescence of Ge-implanted Si/SiO$_2$/Si structures

K. V. Shcheglov, C. M. Yang, K. J. Vahala, and Harry A. Atwater[a)]

Thomas J. Watson Laboratory of Applied Physics, California Institute of Technology, Pasadena, California 91125

Electroluminescent devices were fabricated in SiO$_2$ films containing Ge nanocrystals formed by ion implantation and precipitation during annealing at 900 °C, and the visible room-temperature electroluminescence and photoluminescence spectra were found to be broadly similar. The electroluminescent devices have an onset for emission in reverse bias of approximately −10 V, suggesting that the mechanism for carrier excitation may be an avalanche breakdown caused by injection of hot carriers into the oxide. The electroluminescent emission was stable for periods exceeding 6 h. © *1995 American Institute of Physics.*

The observation of efficient photoluminescence in porous silicon[1] has prompted numerous investigations of optoelectronic properties of nanometer-scale group IV semiconductor clusters.[2] Electroluminescence has been reported for porous silicon during anodic oxidation,[3] and also for porous silicon devices employing thin gold,[4] indium tin oxide,[5] silicon carbide,[6] and polymer contacts.[7] Although porous silicon has motivated considerable interest in nanocrystalline semiconductors, there is interest in other related materials which are more robust in various thermal and chemical ambients, and which can be readily incorporated into a silicon integrated circuit process, or onto substrates other than single-crystal silicon without significant modification of the circuit process technology. A number of alternative synthesis approaches have been reported, ranging from syntheses of nanocrystals in organic solutions from chemical precursors[8,9] to nanocrystals imbedded in an oxide matrix prepared by cosputtering[10,11] or ion implantation.[12,13] The latter approach is quite promising, owing both to the mechanical and chemical robustness of the matrix, as one may expect the nanocrystal-matrix interface to be well passivated from the external ambient, and thus ultimately enabling better control of nonradiative recombination processes which limit luminescence. In addition, the prospects for integration of these materials into existing silicon-based solid state devices and circuits is excellent.

In this letter, we report the use of ion implantation and precipitation to fabricate a Ge nanocrystal-based light-emitting device. Our method for synthesis of Ge nanocrystals in SiO$_2$ consists of ion implantation and precipitation during thermal annealing, a method compatible with existing silicon integrated circuit process technology.[12] In the course of our investigation, it was found that a considerable control over Ge nanocrystal size distribution is possible in the 1–8 nm size range through variation of the Ge implantation dose and annealing conditions. Recently, we have systematically studied the relation of nanocrystal size to luminescence spectral features, but the results suggested that the optical properties of Ge nanocrystals cannot at present be explained adequately by a simple model for quantum confinement of carriers in nanocrystals.[14]

Samples consisted of 45 nm thick polycrystalline Si films deposited initially as amorphous films by ultrahigh vacuum electron beam evaporation onto 70 nm thick SiO$_2$ films thermally grown on n^+ Si substrates. These structures were implanted with Ge at doses of 4×10^{16}/cm^2 at 140 keV, and 1×10^{16}/cm^2 at both 130 and 150 keV. These energies and doses were chosen to create a supersaturated solid solution of Ge in the SiO$_2$ film with approximately uniform Ge concentration of 5 at. % throughout this layer. The samples were subsequently annealed at 600 °C in high vacuum (1×10^{-6} Torr) for 40 min to induce precipitation, then the top layer was doped with B in a furnace at 900 °C for 15 min to generate a p^+ polycrystalline Si film at the top of the structure. Other experiments[14] suggest that Ge nanocrystal growth continued during this 900 °C anneal. Finally, photolithography was used to define isolated mesas for separate devices, and to define Al contacts using liftoff.

Figure 1(a) is a bright-field cross-sectional transmission electron micrograph of the completed device prior to metal contact deposition. Visible at the top is the polycrystalline silicon layer with grain size approximately equal to the film thickness. The top surface of the polycrystalline silicon is very smooth, which is characteristic of films deposited in the amorphous phase and crystallized during a postdeposition anneal. Interface roughness of ~5 nm is observed at the polycrystalline Si/oxide interface, and the thickness of the oxide appears to vary by approximately 5 nm across the field of view of the cross-sectional specimen. Rutherford backscattering spectrometry measurements suggest that the oxide is of a stoichiometry SiO$_x$, where $1.5 \leq x \leq 1.8$. The speckles observable in bright-field contrast correspond to Ge nanocrystals roughly 5 nm in diameter, which are visible in the accompanying dark-field image of the same region shown in Fig. 1(b). The volume density of nanocrystals was approximately 1×10^{18}/cm^3. Also visible is a rough, dark layer at the lower oxide/Si substrate interface, which is probably Ge$_x$Si$_{1-x}$ alloy region which resulted from the extension of the implanted Ge profile at 150 keV into the Si substrate. Also visible is a band of extended defects approximately 100 nm below the oxide/Si interface, which may be due to con-
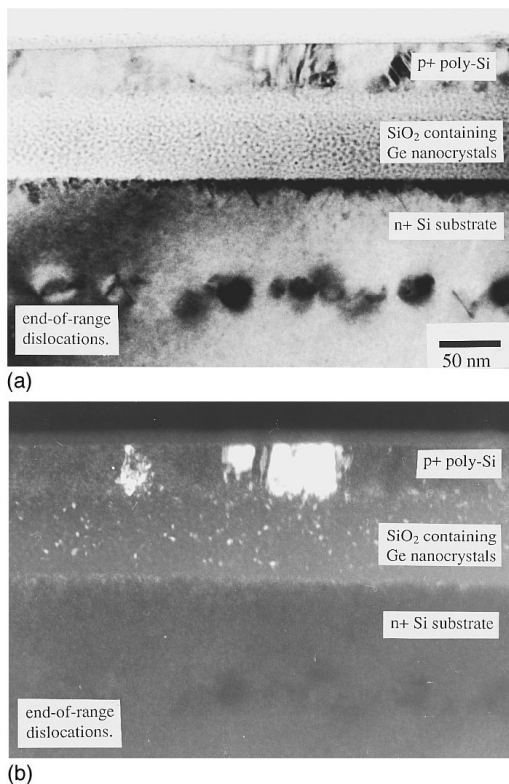
FIG. 1. In (a), a bright-field cross-sectional transmission electron micrograph of the completed device prior to metal contact deposition. In (b), dark-field cross-sectional transmission electron micrograph of the same region.

densation of Si point defects generated from the stopping of ions from the tail of the 150 keV Ge implant profile in the Si substrate.

The individual devices were of various sizes, between 1 and 0.05 mm^2. The devices were electrically characterized with a semiconductor parameter analyzer operating in current-voltage test mode. Electroluminescence was measured with a single grating spectrometer equipped with a charge-coupled device-based optical multichannel analyzer detector. Photoluminescence spectra were measured with the same spectrometer and were pumped with 40 mW of 457 nm radiation from a continuous wave argon ion laser. The system response of the optical spectrometer was carefully calibrated using a blackbody source, and all photoluminescence and electroluminescence raw spectra were divided by the system response curve.

The current-voltage characteristic of a typical device (0.8 mm^2) is shown in Fig. 2. Rectifying behavior is seen in forward bias, and a relatively broad breakdown feature is seen in reverse bias between −5 and −10 V. In both forward and reverse bias, a relatively large series resistance is observed. Electroluminescence is characterized by an onset at reverse bias less than approximately −10 V, which corresponds to an electric field in the oxide of greater than 10^6 V/cm. The dielectric breakdown strength of high-quality, stoichiometric SiO$_2$ is approximately 10^7 v/cm, but the observed breakdown electric field of 10^6 V/cm is reasonable, in view of the modified stoichiometry and structure and of the oxide layer. Device structures fabricated without the Ge ion
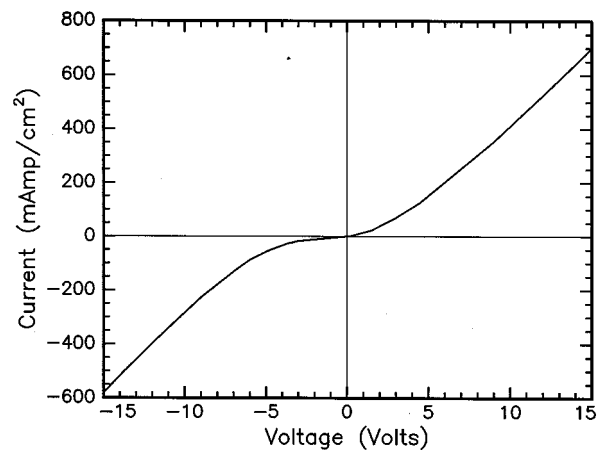

FIG. 2. The current-voltage characteristic of a typical device.

implantation step did not exhibit reverse bias breakdown at voltages less than 50 V, which was the maximum voltage range for the parameter analyzer. The strongly luminescent area usually covered approximately 10% of the device surface. The spatial nonuniformity in emission may be related to nonuniformity in the oxide layer thickness, which would lead to the development of electric fields exceeding the breakdown field in the thinnest oxide regions first. Some of the devices did not exhibit luminescence and their current-voltage traces appeared to be characterized as a diode in series with a large resistance (≥1000 Ω).

The spectra of the devices that did exhibit electroluminescence looked quite similar and were characterized by an emission spectrum with onset at a wavelength of ∼500 nm. Figure 3 is a comparison of photoluminescence spectra. The sharp feature at approximately 510 nm is an artifact generated by division by the system response function, and was related to the abrupt change in transmission of a filter used to suppress the pump beam. We note that there are no artifacts in the spectra at wavelengths above 520 nm, where the filter
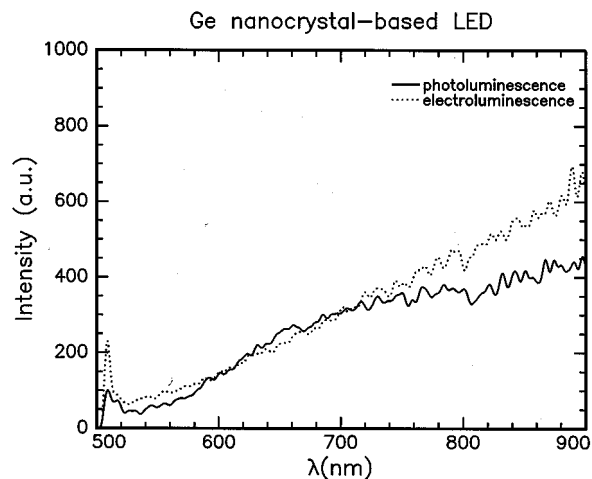

FIG. 3. Photoluminescence and electroluminescence spectra at room temperature for a typical device operating in reverse breakdown. Spectra are corrected for the response of the optical spectrometer. The sharp feature at approximately 510 nm is an artifact of normalization by the spectrometer response function.

Shcheglov *et al.*

transmission is constant and near unity. Differences between the electroluminescence and photoluminescence spectra could have many causes. Possible factors include pump absorption during photoluminescence in the nanocrystal-containing oxide or in the p^+ polycrystalline silicon, and differences in the mechanisms for population of localized states between electrical and optical pumping. The efficiency of electroluminescence (i.e., ratio of optical power out to electrical power in) was difficult to estimate accurately using our current characterization tools, but is probably on the order of 10^{-4}–10^{-5}.

Many important details regarding the mechanism responsible for electroluminescence cannot be deduced from the currently available optical and electrical information, and will require more complete investigation. However, we note that previously investigations of electroluminescence in Si-containing SiO_2 materials that were believed to be broadly similar in morphology to the present structures yielded broadly similar results.[15] Those authors proposed a mechanism based on radiative electronic transitions between discrete energy levels associated with Si islands and/or their interface with the host matrix material. It is possible that carrier injection into these discrete energy states occurs via either relaxation from extended states in the conduction band of SiO_2 or by tunneling from other localized states associated with defects and nanocrystals in the SiO_2 layer. We speculate that the mechanism for excitation of electroluminescence is related to impact ionization by "hot" carriers in the oxide layer, because electroluminescence was observed when the device was in the reverse bias breakdown regime, and no electroluminescence was observed in the forward active region. We note that hot carrier-related electroluminescence is known to occur in reverse bias breakdown in single-crystal silicon,[16] but at much lower efficiencies than reported here.

It is also important to note that emission via blackbody radiation is most likely insignificant for these structures, since visible emission would require local sample temperatures comparable to those employed in the anneals used to precipitate and grow nanocrystals ($\geq 900\,°C$), which would result in significant microstructural and optical changes in the devices during operation. However, no degradation of the electroluminescence intensity was observed after more than 6 h of continuous operation. Moreover, the electrical and optical pump power densities were similar (0.5–5 W/cm^2), and were unlikely to result in enough heating to produce visible blackbody emission from the devices, which were in intimate thermal contact with a 4 cm^2 area, 0.25 mm thick Si substrate.

In summary, a Ge nanocrystal-based light emitting device operating at room temperature has been fabricated using only tools available in a conventional silicon integrated circuit process. Photoluminescence and electroluminescence spectra appeared quite similar. The mechanism for electroluminescence excitation appears to be related to carriers injected in reverse bias breakdown. We anticipate that a better optimized fabrication process may enable injection type luminescence, increased electroluminescence efficiencies, as well as some element of control of the emission wavelength.

[1] L. T. Canham, Appl. Phys. Lett. **57**, 1046 (1990).

[2] V. L. Colvin, M. C. Schlamp, and A. P. Alivisatos, Nature **370**, 354 (1994).

[3] A. Halimaoui, C. Oules, G. Bomchil, A. Bsiesy, F. Gaspard, R. Herino, M. Ligeon, and F. Muller, Appl. Phys. Lett. **59**, 304 (1991); L. T. Canham, W. Y. Leong, M. I. J. Beale, T. I. Cox, and L. Taylor, Appl. Phys. Lett. **61**, 2563 (1992).

[4] N. Koshida and H. Koyama, Appl. Phys. Lett. **60**, 347 (1992); F. Kozlowski, M. Sauter, P. Steiner, A. Richter, H. Sandmaier, and W. Lang, Thin Solid Films **222**, 196 (1992).

[5] F. Namavar, H. P. Maruska, and N. M. Kalkhoran, Appl. Phys. Lett. **60**, 2514 (1992).

[6] T. Futagi, T. Matsumoto, M. Katsuno, Y. Ohta, H. Mimura, and K. Kitamura, Jpn. J. Appl. Phys. **31**, L616 (1992).

[7] K. L. Li, D. C. Diaz, Y. He, J. C. Campbell, and C. Tsai, Appl. Phys. Lett. **64**, 2394 (1994).

[8] W. L. Wilson, P. F. Szajowski, and L. E. Brus, Science **262**, 1242 (1993).

[9] J. R. Heath and F. K. LeGoues, Chem. Phys. Lett. **208**, 263 (1993).

[10] Y. Maeda, N Tsukamoto, Y. Yazawa, Y. Kanemitsu, and Y. Masumoto, Appl. Phys. Lett. **59**, 3168 (1991).

[11] S. Hayashi, T. Nagareda, Y. Kanzawa , and K. Yamamoto, Jpn. J. Appl. Phys. **32**, 3840 (1993).

[12] H. A. Atwater, K. V. Shcheglov, S. S. Wong, K. J. Vahala, R. C. Flagan, M. L. Brongersma, and A. Polman, Mater. Res. Soc. Symp. Proc. **316**, 409 (1994).

[13] T. Shimizu-Iwayama, M. Ohshima, T. Niimi, S. Nakao, K. Saitoh, T. Fujita, and N Itoh, J. Phys. Condens. Matter **5**, L375 (1993).

[14] C. M. Yang, K. V. Shcheglov, K. J. Vahala, and H. A. Atwater (unpublished).

[15] D. J. Dimaria, J. R. Kirtley, E. J. Pakulis, D. W. Dong, T. S. Kuan, F. L. Pesavento, T. N. Theis, J. A. Cutro, and S. D. Brorson, J. Appl. Phys. **56**, 401 (1984).

[16] R. Newman, W. C. Dash, R. N. Hall, and W. E. Burch, Phys. Rev. A **98**, 1536 (1955).